frontiers in Immunology

ORIGINAL RESEARCH
published: 16 April 2021
doi: 10.3389/fimmu.2021.678999

IDO1 Expression in Ovarian Cancer Induces PD-1 in T Cells *via* Aryl Hydrocarbon Receptor Activation

Adaobi Amobi-McCloud[1†], Ravikumar Muthuswamy[1†], Sebastiano Battaglia[1], Han Yu[2], Tao Liu[2], Jianmin Wang[2], Vasanta Putluri[3], Prashant K. Singh[4], Feng Qian[1], Ruea-Yea Huang[1], Nagireddy Putluri[3,5], Takemasa Tsuji[1,6], Amit A. Lugade[1], Song Liu[2] and Kunle Odunsi[1,6,7]*

[1] Center for Immunotherapy, Roswell Park Comprehensive Cancer Center, Buffalo, NY, United States, [2] Department of Biostatistics & Bioinformatics, Roswell Park Comprehensive Cancer Center, Buffalo, NY, United States, [3] Department of Molecular and Cell Biology, Baylor College of Medicine, Houston, TX, United States, [4] Center for Personalized Medicine, Roswell Park Comprehensive Cancer Center, Buffalo, NY, United States, [5] Molecular and Cellular Biology, Advanced Technology Cores, Baylor College of Medicine, Houston, TX, United States, [6] Obstetrics and Gynecology-Gynecologic Oncology, University of Chicago Medicine Comprehensive Cancer Center, Chicago, IL, United States, [7] Department of Gynecologic Oncology, Roswell Park Comprehensive Cancer Center, Buffalo, NY, United States

OPEN ACCESS

Edited by:
Peng Qu,
National Institutes of Health (NIH), United States

Reviewed by:
Darina Ocadlikova, University of Bologna, Italy
Theodoros Eleftheriadis, University of Thessaly, Greece

***Correspondence:**
Kunle Odunsi
odunsia@bsd.uchicago.edu

[†]These authors have contributed equally to this work

Specialty section:
This article was submitted to Cancer Immunity and Immunotherapy, a section of the journal Frontiers in Immunology

Received: 10 March 2021
Accepted: 30 March 2021
Published: 16 April 2021

Citation:
Amobi-McCloud A, Muthuswamy R, Battaglia S, Yu H, Liu T, Wang J, Putluri V, Singh PK, Qian F, Huang R-Y, Putluri N, Tsuji T, Lugade AA, Liu S and Odunsi K (2021) IDO1 Expression in Ovarian Cancer Induces PD-1 in T Cells via Aryl Hydrocarbon Receptor Activation. Front. Immunol. 12:678999. doi: 10.3389/fimmu.2021.678999

The immunoregulatory enzyme, indoleamine 2,3-dioxygenase (IDO1) and the PD-1/PD-L1 axis are potent mechanisms that impede effective anti-tumor immunity in ovarian cancer. However, whether the IDO pathway regulates PD-1 expression in T cells is currently unknown. Here we show that tumoral IDO1 expression led to profound changes in tryptophan, nicotinate/nicotinamide, and purine metabolic pathways in the ovarian tumor microenvironment, and to an increased frequency of PD-1^{+}CD8^{+} tumor infiltrating T cells. We determined that activation of the aryl hydrocarbon receptor (AHR) by kynurenine induced PD-1 expression, and this effect was significantly abrogated by the AHR antagonist CH223191. Mechanistically, kynurenine alters chromatin accessibility in regulatory regions of T cell inhibitory receptors, allowing AHR to bind to consensus XRE motifs in the promoter region of PD-1. These results enable the design of strategies to target the IDO1 and AHR pathways for enhancing anti-tumor immunity in ovarian cancer.

Keywords: IDO, indoleamine 2, 3-dioxygenase, KYN, kynurenine, AhR (aryl hydrocarbon Receptor), PD-1, immunosuppression

INTRODUCTION

Epithelial ovarian cancer (EOC) is the most lethal gynecologic malignancy in the U.S (1). Despite initial response to frontline treatments (i.e. surgery and platinum-based chemotherapy), the majority of patients relapse and ultimately die from their disease within five years (2, 3). Although several studies have demonstrated a positive correlation between EOC prognosis and magnitude of tumor-infiltrating effector T lymphocytes (TIL) (4–6), the clinical benefit of TIL-promoting immunotherapies – such as immune checkpoint inhibitors (ICI), vaccines, and adoptive cell therapy – is limited by the presence of multiple tolerogenic mechanisms within the ovarian tumor microenvironment (TME).

Among several immunosuppressive mechanisms, indoleamine 2,3-dioxygenase (IDO1) has emerged as a key targetable pathway impacting the anti-tumor function of TIL. IDO1 is a heme enzyme which catabolizes the first and rate-limiting step of tryptophan (Trp) catabolism along the kynurenine pathway (KP) to generate active immunosuppressive metabolites. Depletion of tryptophan leads to arrest of T cell proliferation (7), and inducing a stress response *via* activation of the general control nondepressible-2 (GCN2) kinase (8). In addition, kynurenine (Kyn) promotes the differentiation of CD4+ T cells into immunosuppressive regulatory T (Treg) cells *via* activation of the aryl hydrocarbon receptor (AHR) (9, 10). In EOC patients, elevated IDO1 expression correlated with a lower Trp:Kyn ratio in the ovarian tumor microenvironment (11), reduced $CD8^+$ TIL frequency (12), poor prognosis (13, 14), and suppression of T cell responses (15). The vital role of targeting IDO1 for effective immunotherapeutic control of established tumors was observed in pre-clinical models by the synergistic effect of IDO1 inhibition and immune checkpoint inhibitors to mediate the rejection of poorly immunogenic tumors, indicating that IDO1 may be a major mechanism of immunotherapy resistance (16).

Although these observations support therapeutic targeting of the IDO1 pathway, EOC patients treated with epacadostat, an IDO1 inhibitor, did not exhibit objective responses with a median progression-free survival (PFS) of 3.75 months versus 5.56 months for the control group receiving tamoxifen (17). Moreover, a subsequent randomized phase 3 clinical trial in patients with unresectable metastatic melanoma (18) failed to demonstrate improvement in clinical responses when epacadostat was added to pembrolizumab (19–21). These findings suggest that a gap still exists in understanding the full biological consequences of IDO1 enzyme activity in the TME.

Since high IDO1 enzyme activity (11) occurs concomitantly with elevated PD-1 expression on antigen-specific $CD8^+$ T cells as a marker of exhaustion and dysfunction (22), we reasoned that IDO1 may play a role in regulating the expression of PD-1 and other T cell inhibitory receptors in EOC. As the IDO1 metabolite Kyn is an endogenous ligand of AHR transcription factor (23), we investigated a possible role for AHR as the mechanism by which IDO1 facilitates TIL dysfunction associated with inhibitory checkpoint receptor upregulation. In this study, we observed profound IDO1-mediated metabolic and immunoregulatory changes in the ovarian TME, and importantly, induction of inhibitory receptors on $CD8^+$ TIL *via* Kyn-mediated AHR signaling. These data implicate a novel role for Kyn in regulating the exhausted phenotype of $CD8^+$ T cells.

RESULTS

IDO1 Reduces the Prognostic Benefit of TIL in Human EOC and Impacts Overall Survival

We evaluated the clinical outcome of 265 patients with high-grade serous ovarian cancers available in The Cancer Genome Atlas (TCGA) stratified by TIL expression and 44 genes (**Supplemental Table 1**) related to tryptophan catabolism and AHR signaling. TCGA EOC patient cohorts stratified into four distinct populations (TIL^{High}/IDO^{Low}, TIL^{Low}/IDO^{Low}, TIL^{Low}/IDO^{High}, and TIL^{High}/IDO^{High}) (**Figure 1A**). TIL^{High}/IDO^{Low} patients had a significantly improved disease-free survival (DFS) and overall survival (OS) compared with the other groups (**Figure 1B**). Additionally, elevated IDO1 and AHR pathway expression negated the beneficial impact of increased TIL signature (TIL^{High}/IDO^{High} patients), further highlighting a critical role for this pathway. These data suggest that the relationship between IDO1 expression and TIL infiltration is critical in shaping EOC patient outcomes.

To delineate the mechanisms by which IDO1 mediates immune suppression, we generated a stable IDO1-expressing EOC cell line by retroviral transduction (**Supplemental Figure 1A**) of an aggressive ID8 variant, IE9mp1 (24, 25). IE9mp1-mIDO1 tumor cells expressed the murine IDO1 (mIDO1) gene (**Supplemental Figure 1B**) and the gene product demonstrated functional enzyme activity, as measured by elevated Kyn production compared to empty vector (IE9mp1-EV) controls (**Supplemental Figure 1C**). The addition of the mIDO1 gene did not alter *in vitro* cell viability compared with EV control (**Supplemental Figure 1D**). Consistent with the TCGA EOC data, syngeneic wild-type (WT) C57BL/6 mice challenged with IE9mp1-mIDO1 displayed earlier onset of tumor burden (**Figure 1C**) and a significant decrease in overall survival compared with tumors that lack IDO1 expression (**Figure 1D**).

Expression of IDO1 Profoundly Alters the Metabolic Profile of Ovarian Tumors

Dynamic changes in the metabolic profile of intraperitoneal IDO1-expressing ovarian tumors were evaluated by LC-MS measurement of Kyn and its downstream catabolites (26). IDO1 expression at endpoint (Day 47) had the largest effect on the tryptophan, nicotinate/nicotinamide, and purine metabolism pathways ($p<0.05$; Global-ANCOVA) (**Figure 2** and **Table 1**). As expected, IDO1-expressing tumors demonstrated lower levels of tryptophan compared to EV tumors, alongside elevated expression of downstream Kyn metabolites (**Figure 2A**). The metabolite signature also revealed elevation in nicotinic acid, nicotinamide, and quinolinic acid (**Figure 2B**), consistent with enhanced *de-novo* nicotinamide generation *via* the Kyn pathway (27, 28). Nicotinate and nicotinamide metabolites (which include adenosine and thymine) were increased in the IE9mp1-mIDO1 tumors compared with IE9mp1-EV tumors on day 47 (**Figures 2C, D**). Altogether, the impact of tumoral IDO1 expression in ovarian cancer was not only confined to the kynurenine pathway, but also affected nicotinamide, purine and pyrimidine metabolic pathways, and the magnitude of change was influenced by the tumor burden.

Host- and Tumor-Derived IDO1 Expression Drive an Immunosuppressive Cell Profile in the Ovarian TME

To delineate the relative contribution of host- versus tumor-derived IDO1 on the TME immune cell profile, IDO1-sufficient

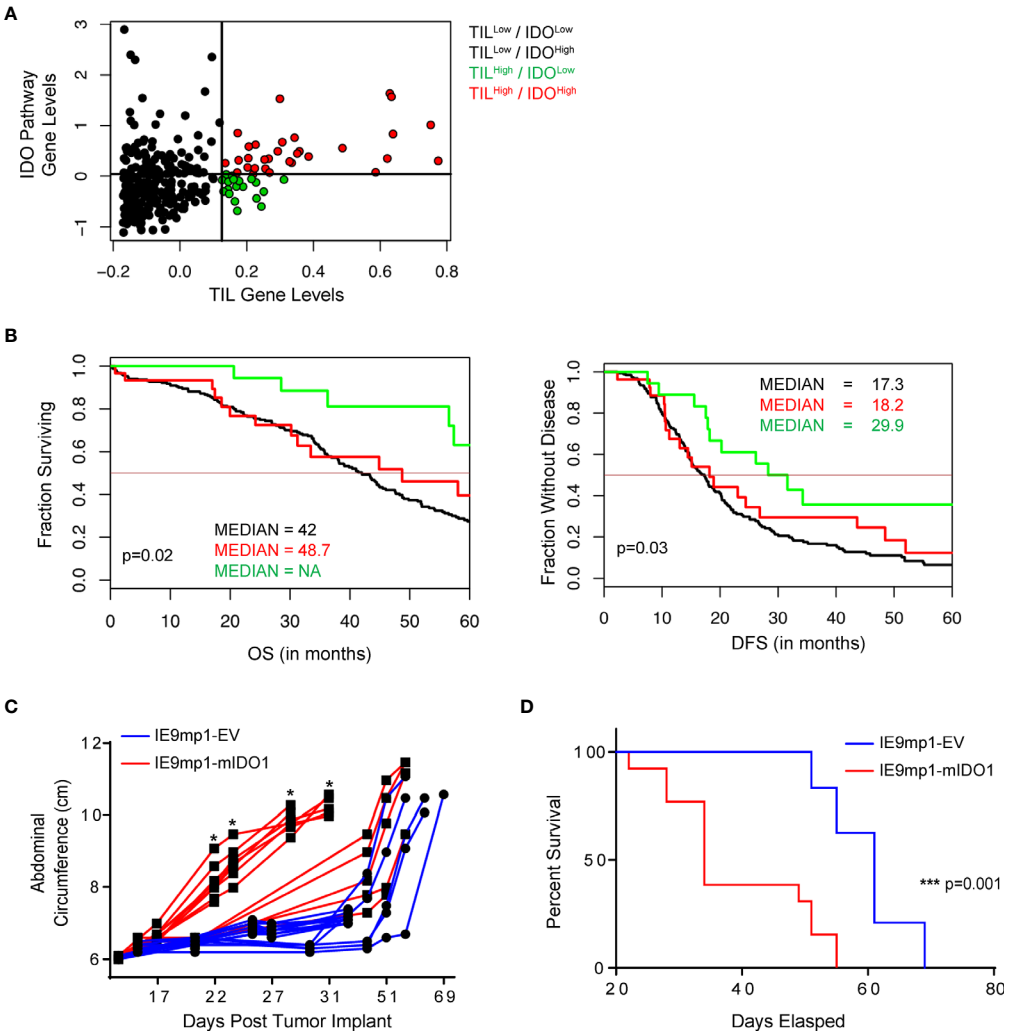

FIGURE 1 | IDO1 reduces the prognostic benefit of tumor infiltrating CD8+ T cells in human ovarian cancer and reduces overall survival in a murine model of ovarian cancer. **(A)** Scatterplot and **(B)** Kaplan-Meier curves of 4 distinct populations comprised of 265 high grade serous ovarian cancer patients from The Cancer Genome Atlas (TCGA) data set. RNA-seq data was analyzed in the context of 44 genes from the tryptophan metabolism and AHR(Aryl Hydrocarbon Receptor) signaling pathways, and CD3E, CD8A, IL2, and Granzyme B. Confidence intervals for the stratified population of patients include OS (Overall Survival): black line median 42.0 [38.0, 46], red line median 48.7[31.2, NA] and green line median NA[57.4, NA] p=0.02; DFS (Disease Free Survival): black line median 17.3[15.1, 19.9], red line median 18.2[13.0, 48.5], and green line median 29.9[18.2, NA] p=0.03). **(C)** 6- to 8- week old WT C57BL/6 mice challenged i.p. with $1x10^7$ IE9mp1-EV (n=10) or IE9mp1-mIDO1 (n=12) tumor cells. Tumor progression was quantified by measuring the abdominal circumference of tumor-bearing mice. **(D)** Kaplan-Meier curves of the survival analysis of IE9mp1-EV (n=14) and IE9mp1-mIDO1 (n=15) tumor-bearing WT C57BL/6 mice. *p < 0.05, ***p < 0.001, by the Log-rank (Mantel-Cox) test **(B, D)**, or Student's t test **(C)**. NA, Not available.

C57BL/6 (WT) mice and IDO1-knockout mice (IDOKO, C57BL/6 background) were challenged intraperitoneally with either IE9mp1-EV or IE9mp1-mIDO1. WT mice bearing IE9mp1-mIDO1 tumors exhibited a non-significant decrease in $CD8^+$ TIL frequency at all time points of tumor growth compared to animals whose tumors lack IDO1 expression (**Figure 3A**, left panel). IDO1 deficient mice also exhibited diminished $CD8^+$ TIL frequency (**Figure 3A**, right panel), but the complete absence of IDO1 expression in tumor and host significantly increased $CD8^+$ TIL frequency on Day 57, indicating that both host- and tumor-derived IDO1 contribute to reduced TIL accumulation in the ovarian TME. Confocal microscopy of IE9mp1-mIDO1 and IE9mp1-EV tumors also confirmed that tumor-derived IDO1 inversely impacted $CD8^+$ TIL frequency (**Figure 3B**).

As IDO1 is known to induce Tregs (8, 10, 29), ovarian TME $CD4^+CD25^+FoxP3^+$ Treg frequency was examined in IDO1-sufficient C57BL/6 mice. Treg frequency was significantly elevated on Day 48 in IE9mp1-mIDO1 tumor-bearing mice (**Figure 3C**) along with increased levels of $CD11b^+Ly6Ghigh$ myeloid cells (**Figure 3D**). To address potential mechanisms regulating the influx and retention of Tregs and myeloid cells in

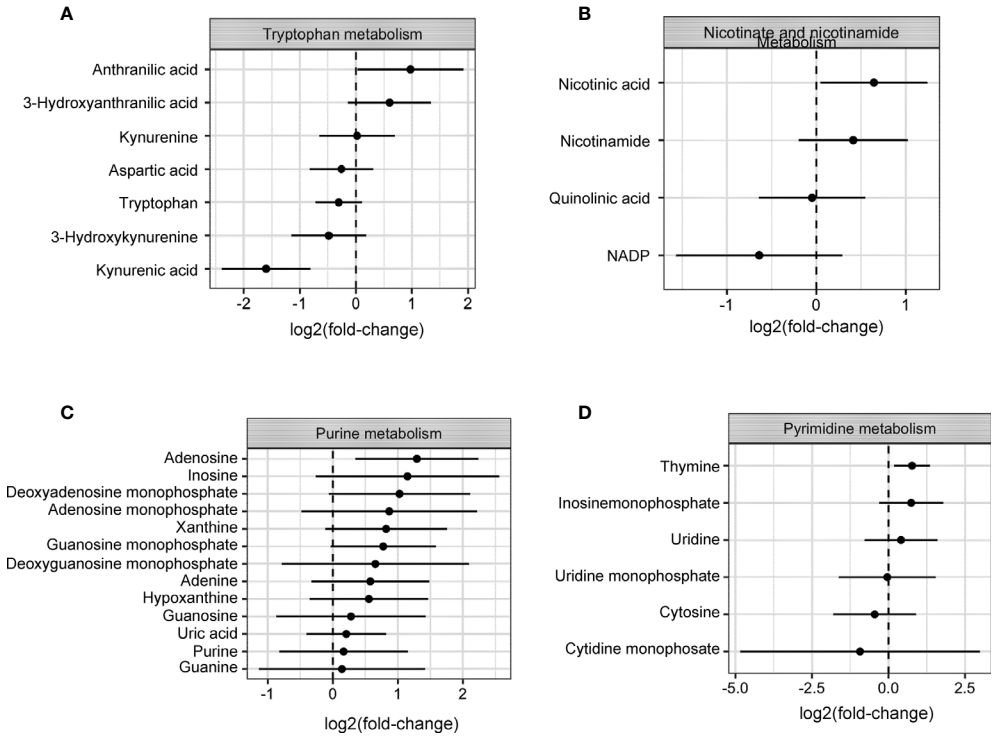

FIGURE 2 | Metabolites levels from the kynurenine, nicotinamide, purine and pyrimidine metabolic pathways are affected by IDO1 expression by the tumor. On Day 28 of tumor progression, whole tumor was harvested from IE9mp1-mIDO1 (n=4) and IE9mp1-Empty Vector control (n=4) tumor-bearing mice. On Day 47 of tumor progression, whole tumor was harvested from IE9mp1-mIDO1 (n=4) and IE9mp1-Empty Vector control (n=5) tumor-bearing mice. Mean log 2 fold changes in metabolites from **(A)** tryptophan amino acid degradation, **(B)** NAD, **(C)** purine and **(D)** pyrimidine metabolism pathways measured in IE9mp1-mIDO1 and IE9mp1-EV tumor from WT C57BL/6 mice on Days 28 and 47. These data presented are the relative abundance measurements of the metabolite level and sample t test statistical analysis reveals the 95% confidence interval of the mean log-fold change in metabolites. The p-values of all the metabolites are listed in **Supplemental Table 1**.

TABLE 1 | Impact of IDO1 on metabolism pathways.

Pathway	p-value	Impact
Tryptophan metabolism	0.003523	0.26445
Nicotinate and nicotinamide metabolism	0.029416	0.1684
Nitrogen metabolism	0.04472	0.00067
Purine metabolism	0.063504	0.20329
Pyrimidine metabolism	0.43918	0.19526

Global-ANCOVA analysis of IE9mp1-mIDO1 or IE9mp1-EV tumor from WT C57BL/6 mice. P-value indicates the significance of overall change for the metabolic pathway in IDO1-expressing tumors. Impact score measures the importance of a metabolite in the metabolic network.

the ovarian TME, chemokines were measured in cell-free tumor ascites fluid from C57BL/6 mice (30). The Treg-attractant MIP-1B/CCL4 (31) was significantly increased in IDO1-expressing tumors (**Supplemental Figure 2A**). Similarly, IDO1-expressing tumors exhibited significant increases in monocyte/macrophage attracting MCP-3/CCL7, eotaxin/CCL11, MCP-1/CCL2, and G-CSF (**Supplemental Figures 2B–E**) (32, 33). These results indicate that tumoral IDO1 expression regulates the ovarian TME chemokine signature for enhanced recruitment of immunosuppressive cells resulting in reduced $CD8^+$ TIL frequency.

Kynurenine Mediates Induction of Inhibitory Receptors on $CD8^+$ T Cells

To assess whether host- or tumor-derived IDO1 expression leads to upregulation of inhibitory receptors, we analyzed the phenotype of $CD8^+$ TILs isolated from WT and IDOKO mice bearing either IE9mp1-mIDO1 or IE9mp1-EV tumors. In both IDO1-sufficient and IDO1KO TIL, tumoral IDO1 expression significantly increased the frequency of PD-1^+ $CD8^+$ TIL on Day 48 compared with those from IE9mp1-EV challenged mice (**Figure 4A**). Notably, in the absence of host- and tumor-derived IDO1 this effect was abrogated and there was no significant upregulation of PD-1 on $CD8^+$ TIL at the same time point (Day 48) in IE9mp1-EV tumor-bearing IDOKO mice, indicating that regardless of the cellular source of IDO1 expression, presence of IDO1 enzyme activity contributes to PD-1 upregulation on ovarian $CD8^+$ TIL.

The contribution of IDO1-induced KYN generation by tumor cells on PD-1 expression was evaluated using anti-CD3/anti-CD28 activated $CD8^+$ lymphocytes. IE9mp1-mIDO1 cell culture supernatant allowed for a controlled system where IDO1-mediated Trp catabolism into KYN could be quantified (**Figure 4B**, left). $CD8^+$ T cells significantly upregulated PD-1 expression in the presence of elevated tumor-produced KYN

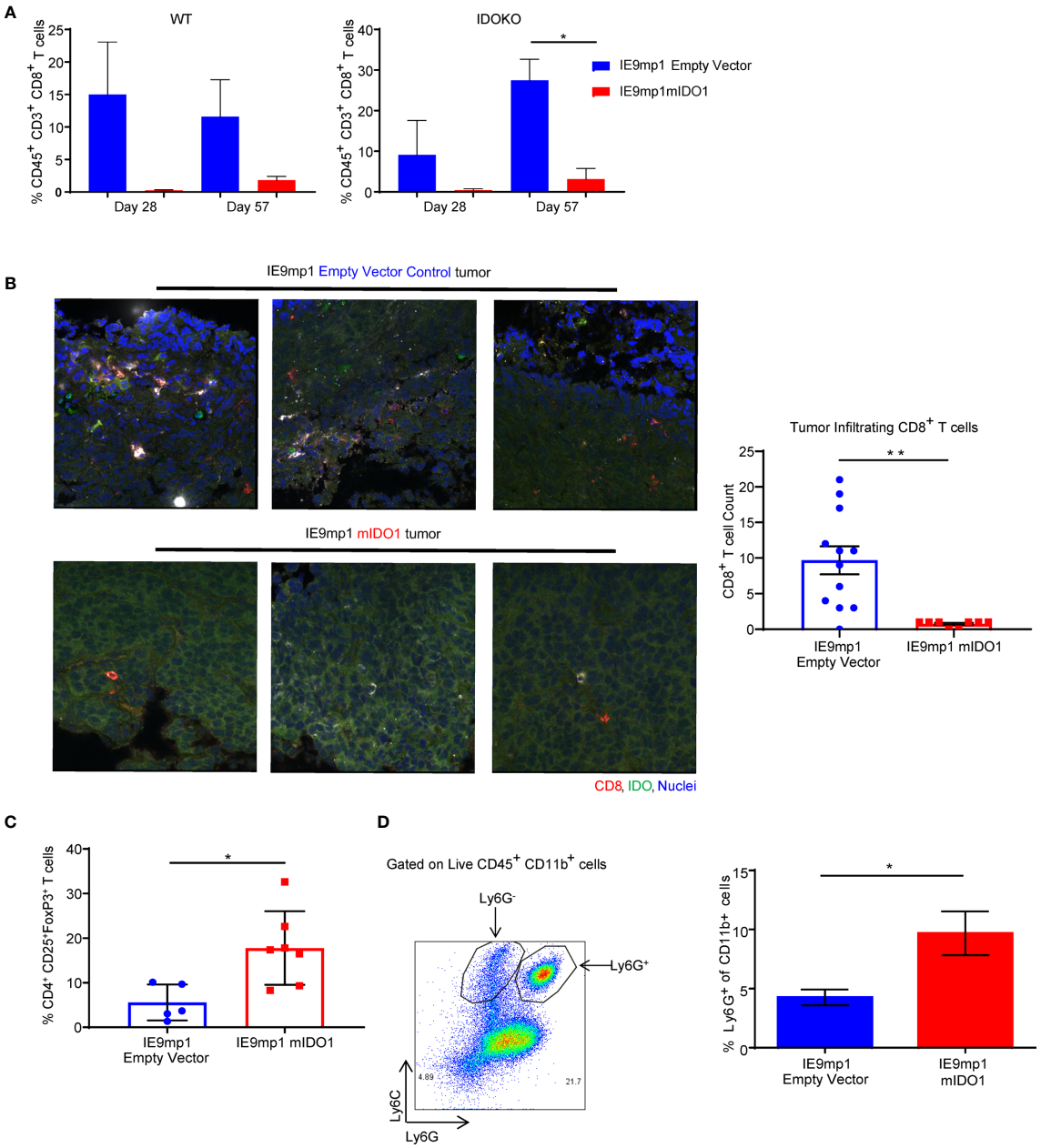

FIGURE 3 | Expression of IDO1 leads to poor tumor infiltration by CD8+ T cells and increased infiltration of suppressive immune cells in the ovarian tumor microenvironment. **(A)** Frequency of CD8+ TILs on Days 28 and 57 from WT C57BL/6 (left panel n=6) and IDOKO (right panel n=6) mice challenged i.p. with 1x10e7 IE9mp1-mIDO1 or IE9mp1-EV tumor cells. **(B)** Immuno-stained IE9mp1-mIDO1 and IE9mp1-EV tumor from WT C57BL/6 mice on Day 48 with anti-IDO1 (green), CD8+ T cell (red), and DAPI (blue). Quantification of CD8+ T cells from 3 field images per tissue slide, (n=11 IE9mp1-EV and n=8 IE9mp1-mIDO1). Total original magnification is 63x. **(C)** Flow cytometry analysis of tumor ascites for $CD4^+CD25^+FoxP3^+$ T cell frequency in IE9mp1-mIDO1 (n=7) and IE9mp1-EV (n=5) tumor-bearing WT C57BL/6 mice on Day 48. **(D)** Frequency of Ly6G+in $CD11b^+$ cell IE9mp1-EV (n=5) or IE9mp1-mIDO1 (n=5) tumor-bearing WT C57BL/6 mice on Day 28. *p < 0.05, **p < 0.01, using Student's t test **(B–D)**. The data represent means ± SEM of three independent experiments.

(**Figure 4B**, right). Activation of $CD8^+$ T cells in varying KYN concentrations resulted in upregulation of not only PD-1 (**Figure 4C**), but also additional inhibitory receptors such as *Klrg1* (**Figure 4D**) and *Tim3* (**Figure 4E**), although the effect was more pronounced at higher KYN concentrations. Taken together, these results demonstrated that kynurenine contributed to the upregulation of co-inhibitory receptors expression on CD8+ T cells *in vivo* and *in vitro*.

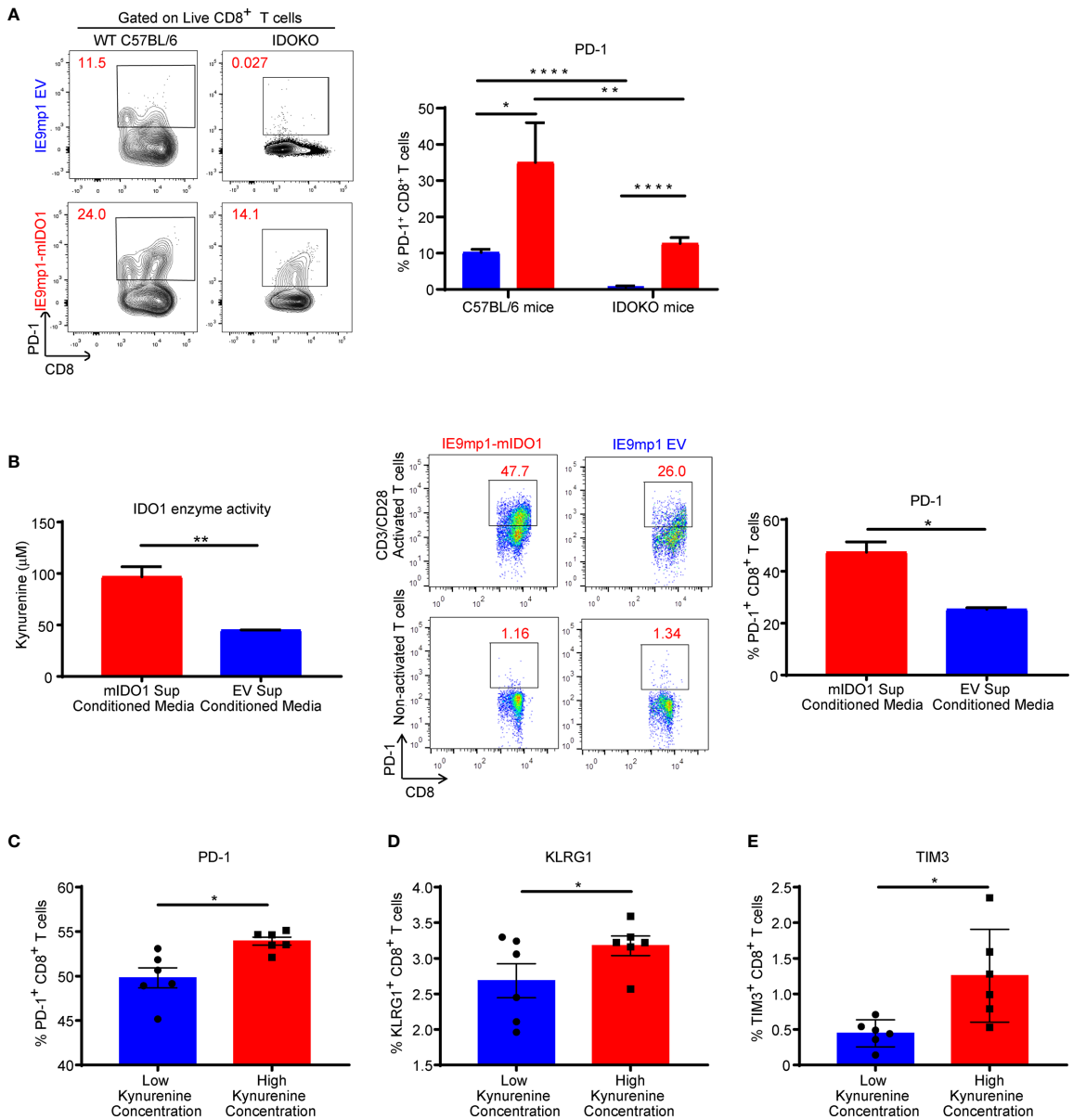

FIGURE 4 | Kynurenine mediates upregulation of inhibitory receptor on CD8+ T cells. **(A)** Frequency of PD1+CD8+ T cells in tumor ascites from WT C57BL/6 or IDOKO mice challenged i.p. with 1x10e7 IE9mp1-EV (n=5) or IE9mp1-mIDO1 (n=6) tumor cells on Day 48, as determined by flow cytometric analysis. (**B**, left) Kynurenine concentrations measured in IE9mp1-EV and IE9mp1-mIDO1 tumor cell culture supernatant by colorimetric assay. (**B**, right) Frequency of PD1+CD8+ T cells, from WT C57BL/6 mice spleens, co-cultured with 1μg/mL anti-CD3/CD28 in IE9mp1-mIDO1 or IE9mp1-EV tumor cell culture supernatant for 48 hr. PD1+CD8+ T cell frequency was determined by flow cytometric analysis. **(C)** PD-1, **(D)** KLRG1, and **(E)** TIM3 expression analyzed by flow cytometric analysis on T lymphocytes from WT C57BL/6 mice activated with 1μg/mL anti-CD3/CD28 and with treated kynurenine. *p < 0.05, **p < 0.01, ****p < 0.0001, by Student's t test **(A–E)**. The data represent means ± SEM of three independent experiments performed in triplicate.

PD-1 Gene Contains Putative AHR Binding Sites

Upon activation by its natural endogenous agonist, KYN, AHR translocates into the nucleus and regulates target gene expression in T cells (9, 10), including a tumor-promoting role *via* suppression of anti-tumor immunity (23). To account for this observation, we hypothesized that the genes encoding T cell inhibitory receptors contain AHR binding sites responsible for transcriptional regulation upon sequential KYN ligation and AHR activation. Therefore, we performed computational analysis of promoter regions of T cell inhibitory receptor genes for the consensus AHR xenobiotic response elements (XRE) binding motifs (**Figure 5A**). We identified multiple AHR binding sites in the upstream gene promoter region of murine

(**Figure 5B**) and human *Pdcd1* (PD-1) gene (**Supplemental Figures 3** and **4**). AHR binding sites were also present in the upstream promoter regions of additional inhibitory receptors such as *Lag3*, *Tim3*, *Klrg1*, *Ctla4*, *Btla*, *2B4*, *CD160* and *TIGIT* (**Supplemental Figures 3** and **4**).

To address the mechanism by which KYN mediates PD-1 expression, we next evaluated AHR expression in activated $CD8^+$ T cells. AHR gene expression in T cells was not altered by their activation in the presence of KYN or another well characterized exogenous AHR ligand, 2,3,7,8-tetrachlorodibenzo-p-dioxin (TCDD) (**Figure 5C**) (34). Although KYN ligation did not impact AHR expression in T cells, it did result in AHR target gene transcription, specifically the cytochrome P40 enzyme, *Cyp1a1* (**Figure 5D**) (35), confirming KYN-mediated AHR activation. As *Cyp1a1* expression requires nuclear translocation of the active AHR-KYN complex (36, 37), we evaluated the kinetics of KYN-mediated AHR nuclear translocation in activated $CD8^+$ T cells. At 2 hours post-activation in the presence of KYN and TCDD, AHR was observed in the nucleus (**Figure 5E**, green) and thus provides a mechanism by which AHR directly mediates PD-1 expression in $CD8^+$ T cells.

Kynurenine Permits Genome-Wide Chromatin Accessibility In Regulatory Regions of PD-1 Gene

As KYN-mediated upregulation of inhibitory receptors requires AHR interaction with XRE sequences in the promoter regions, we next evaluated how KYN treatment alters the dynamics of $CD8^+$ T cell genome-wide chromatin accessibility by ATAC-seq (38). Increases of chromatin accessibilities in KYN-treated activated $CD8^+$ T cells were observed for two regulatory elements of the *Pdcd1* (**Figure 6A**) and *Lag3* (**Supplemental Figure 5**) genes, indicating that KYN treatment mediates the extent of chromatin accessibility for key T cell inhibitory receptors leading to their upregulation. Moreover, these data also suggest an epigenetic role for IDO1 in regulating the transcriptional activity of $CD8^+$ TIL.

KYN Induces PD-1 Expression on $CD8^+$ T Cells in an AHR-Dependent Manner

Direct evidence for KYN-mediated AHR binding to XRE motifs in the PD-1 promoter was evaluated by chromatin immunoprecipitation of activated $CD8^+$ T cells (**Supplemental Figure 6**). ChIP-qPCR using anti-AHR bound to genomic DNA confirmed enrichment of AHR binding to XRE motifs within the murine *Pdcd1* gene promoter region by KYN treatment but not by TCDD (**Figure 6B**). Furthermore, ChIP-qPCR verified PD-1 gene expression was upregulated in the presence of KYN. The requirement for AHR-mediated PD-1 expression following KYN treatment was tested by utilizing the AHR antagonist CH223191 (39). In addition to inhibiting its downstream target gene *Cyp1a1*, AHR antagonism severely diminished KYN-mediated PD-1 upregulation on $CD8^+$ T cells (**Figures 6C, D**). These data confirm that AHR interaction with responsive elements in the PD-1 promoter facilitates its transcription upon treatment with KYN and suggests an approach in which AHR antagonism can be coupled with IDO1 blockade to synergistically prevent PD-1 mediated T cell dysfunction.

DISCUSSION

Tryptophan catabolism by IDO1 has been firmly established as a powerful mechanism of innate and adaptive immune tolerance in EOC and other solid tumors (13, 14, 16, 40). However, efforts to target this pathway in the clinic has met with limited success (17, 18), probably because the full biologic consequences of IDO1 on the TME remain incompletely characterized. In this study, we fill a major gap in knowledge by demonstrating that (1) the metabolic re-wiring of the TME by IDO1 is profound and goes beyond KYN accumulation by also affecting nicotinate/nicotinamide and purine metabolism; (2) KYN differentially alters frequencies of CD8 T vs regulatory T cells (Treg)/Myeloid derived suppressor cells (MDSC) cells in tumor; (3) KYN alters chromatin accessibility in regulatory regions of inhibitory receptors leading to their upregulated expression; and (4) AHR binding to consensus XRE motifs is the mechanism by which IDO1 activity mediates T cell dysfunction. These results support the design of strategies to target the IDO1 and AHR pathways for improving anti-tumor immunity in EOC. While we focused here on the impact of IDO1 on adaptive immunity, its tumor intrinsic role would need to be clarified in future studies.

To study the consequences of the metabolic microenvironment imposed by IDO1, we first investigated quantitative and qualitative changes in $CD8^+$ T cell infiltration. In addition to the effect of IDO1 in reducing intra tumoral accumulation of $CD8^+$ TIL, the cytokine milieu of the TME was noted to favor the recruitment of immunosuppressive Tregs and myeloid cells. Tumoral IDO1-induced KYN was sufficient to upregulate PD-1 on $CD8^+$ T cells *in vivo* and *in vitro*. Moreover, we established AHR activation by KYN as the mechanism by which $CD8^+$ T cells acquired an exhausted phenotype of PD-1 expression.

Although our bioinformatics analyses identified AHR XRE binding sites in the promoter region of several human and murine checkpoint receptor genes, chromatin accessibility by ATAC-seq indicated the potential for AHR transcription factor occupancy in *Pdcd1* and *Lag3* of inhibitory receptor genes. Since ATAC-seq alone cannot decide which transcription factor binds to accessible chromatin (38), we utilized ChIP-qPCR and demonstrated specific binding of AHR to DNA in the *Pdcd1* gene. Thus, KYN increased the accessibility of AHR to XRE sequences in the PD-1 gene promoter of $CD8^+$ T cells. Further support for an AHR-dependent mechanism for kynurenine upregulation of PD-1 gene expression is provided by abrogation of gene expression in the presence of the AHR antagonist CH223191. These findings establish that kynurenine activation of AHR is a critical mechanism by which IDO1 impacts the upregulation of checkpoint receptors on $CD8^+$ T cells in the ovarian TME. Although PD-1 expression was shown to be mediated by non-physiological concentrations of KYN in a recent study (41), the downstream transcriptional events that regulate this

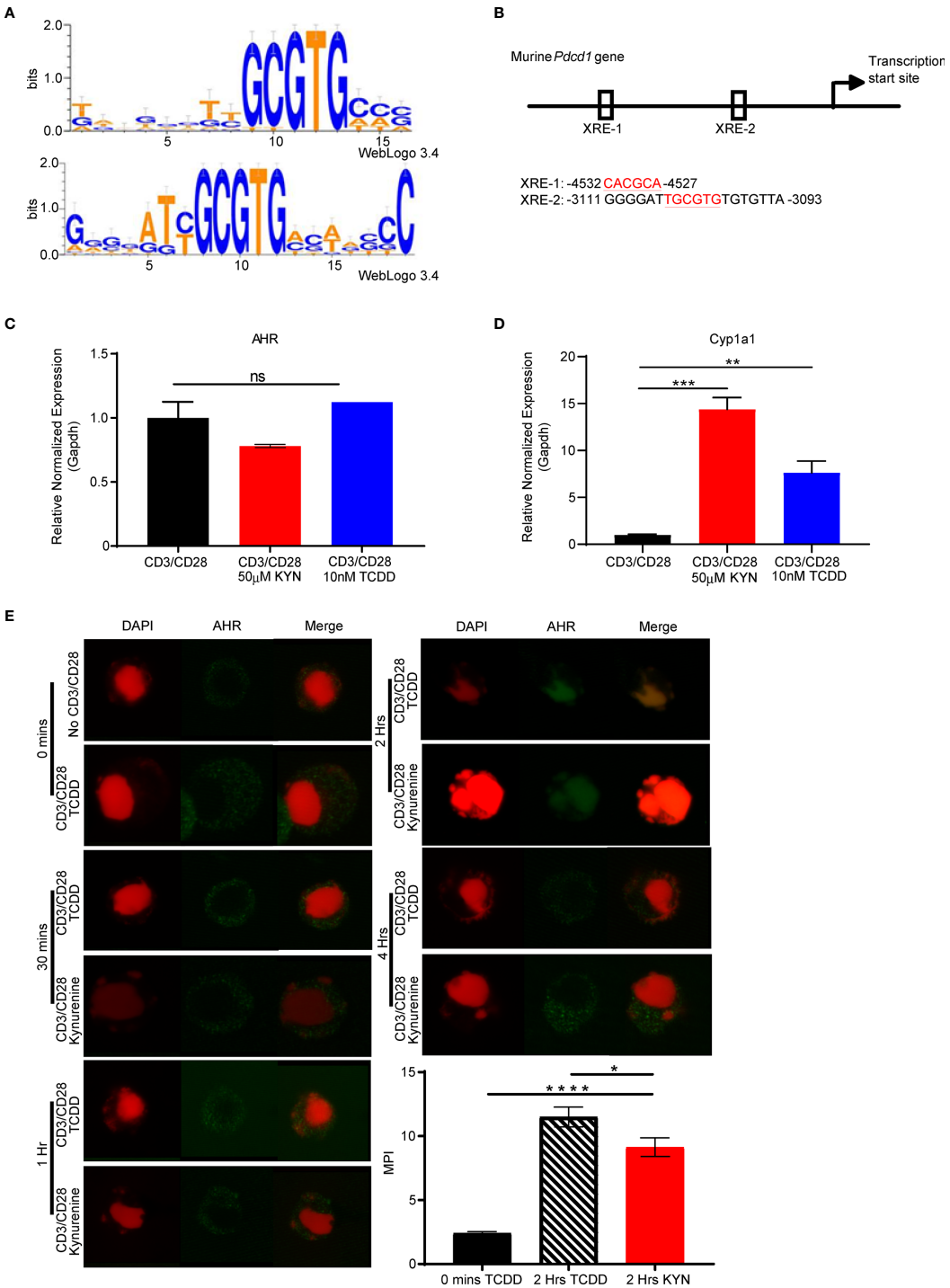

FIGURE 5 | PD-1 gene contains putative aryl hydrocarbon receptor binding sites. **(A)** Motif Logo depicting the position specific weight matrices of the AHR binding site [xenobiotic response element (XRE)]. **(B)** Schematic representation of the identified AHR binding site in the *Pdcd1* promoter. **(C)** Anti-CD3/CD28 activated CD8+ T cells from spleens of WT C57BL/6 mice were treated with IL-2 (50U/mL), KYN (50μM) or TCDD (10nM) for 6 days. AHR and **(D)** *Cyp1a1* mRNA was determined. **(E)** AHR nuclear translocation was measured in anti-CD3/CD28 bead-activated CD8+ T cells from spleens of WT C57BL/6 mice treated with KYN (50μM) or TCDD (10nM) for 0,0.5,1,2 and 4hrs as indicated. CD8+ T cells were immuno-stained for AHR (green) and DAPI (red). Mean pixel intensity (MFI) of AHR nuclear translocation was calculated (bar graph) using Image J Total original magnification is 189x. *$p < 0.05$, **$p < 0.01$, ***$p < 0.001$, ****$p < 0.0001$, ns, not significant, by Student's t test **(D, E)**. The data represent means ± SEM of three independent experiments performed in triplicate.

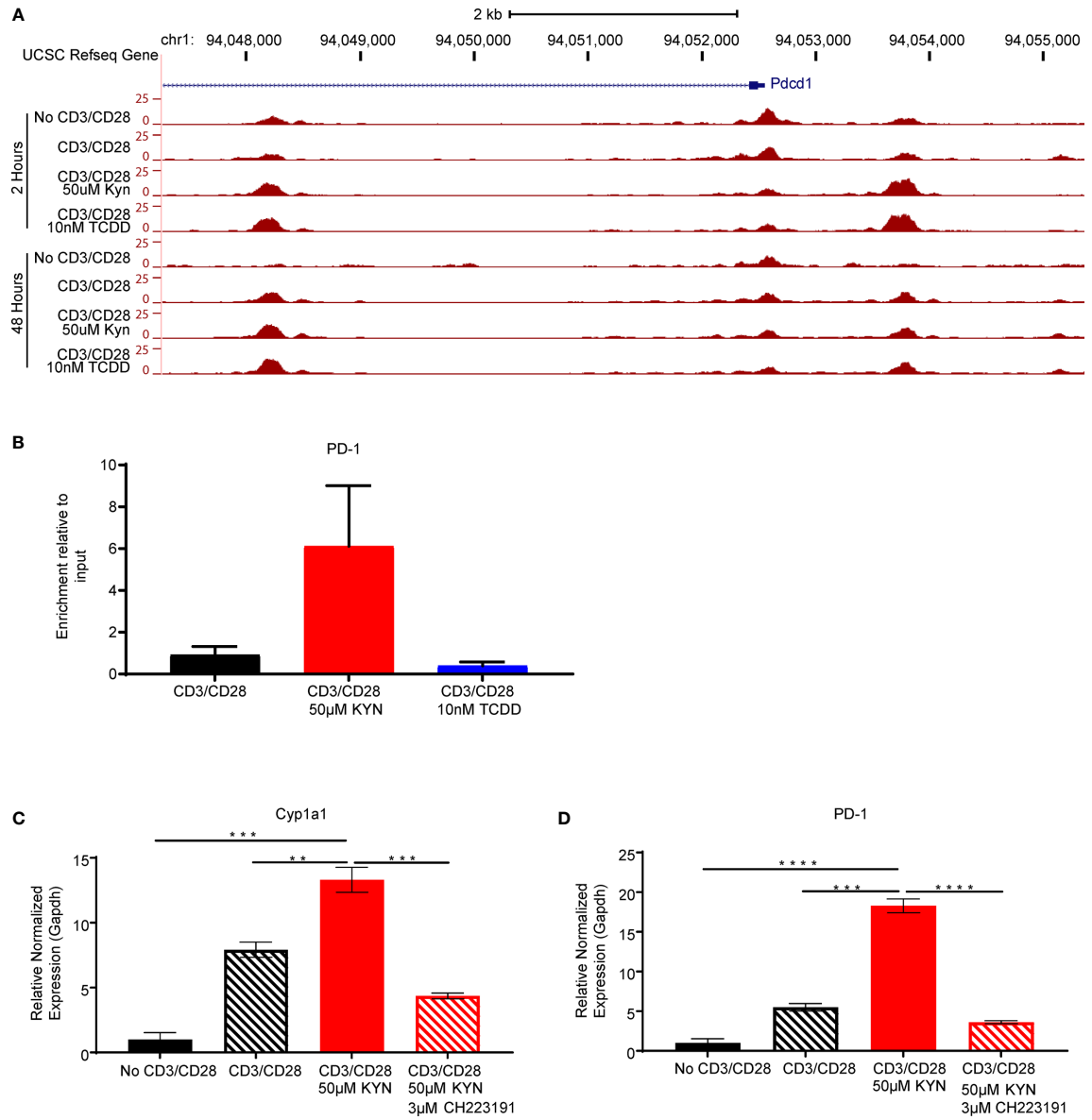

FIGURE 6 | Kynurenine induces PD-1 expression on CD8+ T cells in an AHR-dependent manner. **(A)** UCSC Genome Browser plot of open chromatin accessible regions in two DNA regulatory elements in the PD1 gene identified by ATAC-seq analysis of CD8+ T cells, from WT C57BL/6 mice, activated by anti-CD3/CD28 and treated with KYN (50μM) or TCDD (10nM) for 2 and 48 hrs. **(B)** CHIP-qPCR *Pdcd1* analysis in anti-CD3/CD28 bead-activated and KYN (50μM) treated CD8+ T cells for 2 hours from spleens of WT C57BL/6 mice with AHR antibody and *pdcd1* promoter primers. **(C)** Anti-CD3/CD28 activated CD8+ T cells from spleens of WT C57BL/6 mice were treated with KYN (50μM) and CH223191(AHR antagonist) (3μM) for 6 days. *Cyp1a1* and **(D)** PD-1 mRNA was determined. $^{**}p < 0.01$, $^{***}p < 0.001$, $^{****}p < 0.0001$ by Student's t test **(B–D)**. The data represent means ± SEM of three independent experiments performed in triplicate **(B–D)**.

dysfunctional TIL phenotype were not identified. Our study provides a targetable mechanism by which IDO1 regulates inhibitory checkpoint receptors on $CD8^+$ TIL *via* kynurenine activation of AHR.

A notable limitation of the present study is that while we have uncovered alterations in metabolic pathways beyond kynurenine, their contribution to induction of T cell inhibitory receptors or other mechanisms of immune suppression were not fully examined. For example, NAD is able to regulate CD4 T cell differentiation and promotes IL-10 and TGF-B1 production by Th1 and Th17 cells, respectively (42). In addition, it will be important to confirm whether AHR mediated upregulation of inhibitory T cell receptors is a general mechanism for other metabolites along the kynurenine pathway. Moreover, while murine studies can yield valuable insights into AHR function, there are differences between the human and mouse AHR, such as differences in the affinity to ligand activation (43) indicating that future human studies will need to be conducted with this caveat in mind. In addition, a report by

Eleftheriadis et al. (44) indicated that IDO decreased glycolysis and glutaminolysis by activating GCN2K, and IDO–induced activation of AhR increased the expression of all carnitine palmitoyltransferase I isoenzymes, leading ultimately to increased free fatty acid (FFA) oxidation and preservation of $CD4^+$ T–cell survival and proliferation. This implies that in a normal environment containing fatty acids, $CD4^+$ T–cell survival and proliferation may not be reduced since IDO-mediated supply of FFA would provide the required energy for cell survival and proliferation. Since this was not a focus of our study, future studies are warranted to examine the potential impact of any IDO-mediated effects on FFA generation on CD4+ T cells. We acknowledge that these results are described in an overexpressing IDO1 tumor model. Intrinsically, parental ID8 tumor cells do not produce appreciable levels of IDO1 (data not shown), therefore, we generated a stable IDO1-expressing EOC cell line by retroviral transduction. Also, ID8 by its nature is not a typically inflammatory tumor model, however, we show in these studies that the TILs that enter the tumor can be modulated by IDO1 and has an impact on efficacy.

Despite these limitations, our current study sheds some light on potential reasons for the limited efficacy of ECHO-301/KEYNOTE-252 (NCT02752074), the first phase 3 randomized double-blind study of epacadostat in combination with anti-PD-1 antibody pembrolizumab in patients with unresectable or metastatic melanoma (19–21). First, KYN activation of AHR may be a major resistance mechanism *via* upregulation of several immune checkpoint receptors, with the implication that PD-1 blockade monotherapy may be insufficient to derive benefit from IDO1 blockade. We demonstrate that *Lag3* gene expression on $CD8^+$ TILs are similarly impacted by KYN, and therefore *Lag3* may serve as a compensatory escape pathway when the PD-1/PD-L1 pathway is blocked. Second, the impact of tumoral IDO1 expression in ovarian cancer was not confined to the kynurenine pathway, but also mediated metabolic changes downstream of kynurenine, demonstrating a role for nicotinate, nicotinamide, purine and pyrimidine metabolic pathways. Lastly, AHR antagonists have been identified and examined as potential therapeutic tools to study the role of AHR in tumorigenesis (34). Preclinical studies in multiple myeloma, suggest that therapeutic targeting of the AHR, with an inhibitor such as the FDA-approved clofazimine (45), may improve clinical outcomes.

Altogether, this study demonstrates that IDO1-induced KYN activates AHR nuclear translocation where its direct binding to XRE motifs in the PD-1 gene promoter (**Supplemental Figure 7**) results in T cell dysfunction. Strategies to concomitantly target the IDO1 and AHR pathways may overcome immune suppression and enhance anti-tumor immunity in EOC and other solid tumors.

METHODS

The Cancer Genome Atlas (TCGA) Data Analysis

Gene expression data were downloaded from cBioportal. Immune and IDO signature scores were calculated using the sum of the gene expression selected genes (**Supplemental Table 1**) divided by the square root of the number of genes. Patients were then divided in four groups: TIL^{High}/IDO^{Low}, TIL^{Low}/IDO^{Low}, TIL^{Low}/IDO^{High}, and TIL^{High}/IDO^{High} based on immune and IDO score values. Survival analysis across groups was calculated using clinical information available on cBioportal using log rank test at a significance threshold of 0.05.

Animals. Female and male WT C57BL/6 mice and IDOKO mice (stock no. 005867) were purchased from Jackson Laboratory (Bar Harbor, ME), and bred in our facility (Roswell Park Comprehensive Cancer Center) according to an approved protocol. All animals were maintained in the Laboratory Animal Shared Resource under specific pathogen-free conditions. All animal experiments were carried out according to protocol guidelines approved by the Institute Animal Care and Use Committee (IACUC) of Roswell Park Comprehensive Cancer Center (Buffalo, NY).

Cell Lines. The murine *Ido1* (mIDO1) gene was overexpressed in mouse ovarian surface epithelial cell (MOSEC) lines by retroviral transduction. Full-length mIDO1 gene was PCR amplified from cDNA of IFNG treated ID8 cell line (25) and inserted into the first cloning site in a retrovirus backbone vector (pQCXIX, Clontech-TaKaRa). A fusion gene of codon-optimized Luciferase (Luc2) and tandem-dimeric Tomato (tdT) gene was PCR amplified from the pcDNA3.1(+)Luc2=tdT (Addgene plasmid # 32904) (a gift from Christopher Contag at Stanford University, Stanford, California) (46) and inserted into the second cloning site. The parental IE9 cell line was provided to our lab by Dr. Tahiro Shin at the University of Texas Health Sciences Center (San Antonio, Texas). A control empty vector was constructed by inserting Luc2=tdT gene alone. The retroviral transfer vector was co-transfected with pVSV-G retroviral envelope-expressing plasmid into the GP2-293 cell line (Clontech-TaKaRa) using Lipofectamine 2000 reagent (Invitrogen) to produce retrovirus supernatant. Parental ID8 (25), IE9 (47) or IE9mp1 (24) tumor cell lines were transduced by retroviral vectors in the presence of 8mg/ml polybrene (Sigma-Aldrich). Stable cell lines were established after flow cytometry cell sorting of tdT-expressing cells using a FACSAria 2 (BD Biosciences). Expression of tdT in established cell lines was periodically monitored by flow-cytometry and confirmed that >99% cells expressed tdT before experiments. All cell lines were cultured in complete culture medium: RPMI1640 (Corning Cellgro®) supplemented with 10% fetal bovine serum (VWR), 1% sodium pyruvate (100mM), 1% L-glutamine (200mM), 1% MEM nonessential amino acid (100x), 1% penicillin/streptomycin (100x), 2.5% Hepes, and 0.1% beta-2-mercaptoethanol (50mM) in an incubator at 37°C and 5% CO_2.

Tumor Challenge and Measurement

WT C57BL/6 and IDOKO mice were challenged intraperitoneally (i.p.) with $1x10^7$ IE9mp1-mIDO1 or IE9mp1-EV tumor cells in a final volume of 500µl Dulbecco's PBS (Corning Cellgro®). Tumor progression and the amount of tumor burden were monitored by measuring abdominal distension to track the accumulation of peritoneal ascites formation. Mice were euthanized by CO_2 asphyxiation and/or

cervical dislocation when the abdominal circumference of i.p. tumors reached a 50% girth increase and/or upon detection of declining health conditions as described in our standard operating procedure for Body Scoring, according to IACUC guidelines.

IDO Enzyme Activity Measurement

Kynurenine was measured in cell culture supernatants by incubating the sample with a 30% w/v Trichloroacetic acid (Sigma-Aldrich) solution prepared in water, and Ehrlich reagent (2% PDAB) prepared fresh for each assay by dissolving p-dimethylaminobenzaldehyde (PDAB) (Sigma-Aldrich) in acetic acid. The colorimetric reaction was measured using a microplate reader at OD 490nm. The OD values were measured and calculated against standard dilution curve of L-kynurenine (Sigma-Aldrich).

Flow Cytometry Antibodies and Reagents

LIVE/DEAD™ Fixable Yellow Dead Cell Stain Kit, for 405nm excitation catalog no. L34959 was purchased from Thermo Fischer Scientific. Mouse-specific FITC-anti-CD45 (clone 30-F11) catalog no.11-0451-82, eFluor 450-anti-CD11b (clone M1/70) catalog no. 48-0112-82, APC-anti-TIM3 (clone 8B.2C12) catalog no. 17-5871-80, APC-anti-CD25 (clone PC61.5) catalog no.17-0251-82, PerCP-eFluor 710-anti-CD8A (clone 53-6.7) catalog no.46-0081-82, PE-anti-Foxp3 (clone FJK-16s) catalog no. 12-5773-82, and PE-Cy7-anti-CD4 (clone GK1.5) catalog no. 25-0041-82 were purchased from eBiosciences. BV421-anti-PD-1 (clone 29F.1A12) catalog no. 135218 was purchased from BioLegend. Anti-CD16/CD32 FcBlock (clone 2.4G2) catalog no.553142, PE-Cy7-anti-Ly6G/Ly6C (clone RB6-8C5) catalog no.565033, BV450-anti-CD45 (clone 30-F11) catalog no. 560501, FITC-anti-CD8A (clone 53-6.7) catalog no. 553031, PerCP-Cy5.5-anti-Ly6G/Ly6C (clone RB6-8C5) catalog no. 561103, PerCP-anti-CD8A (clone 53-6.7) catalog no.553036, PE-anti-CD3E (clone 145-2C11) catalog no.553064, PE-anti-CD11b (M1/70) catalog no. 557397, and PerCP-anti-CD4 (clone RM4-5) catalog no. 553052 were purchased from BD Biosciences. Foxp3/Transcription Factor Fixation and Permeabilization Concentrate and Diluent kit, catalog no. 00-5523-00 (eBiosciences) was used for intracellular Foxp3 staining. Flow cytometry data were acquired using a BD Biosciences LSR 2 flow cytometer and BD FACSDiva software, and analyzed using FlowJo v10 software (TreeStar).

RNA Isolation and Quantitative Real-Time Polymerase Chain Reaction (PCR) Analysis

Total RNA was isolated using the RNeasy mini kit (Qiagen). cDNA was prepared using iScript cDNA Synthesis kit (BioRad) and reverse transcription was carried out on the T100 Thermal Cycler (BioRad). Quantitative real-time PCR was performed using iQ SYBR Green Supermix (BioRad) on the C1000 Touch Thermal Cycler, CFX96 Real-Time System (BioRad). Primer sequences used include *Ido1* forward 5'-TCTGCCTGTGC TGATTGA-3', reverse, 5'-CTGTAACCTGTGTCCTCTCA-3'; *AHR* forward 5'-CCACTGACGGATGAAGGA-3', reverse, 5'-ATCTCGTACAACACAGCCTCT-3'; *CYP1A1* forward 5'-GACACAGTGATTGGCAGAG-3', reverse, 5'-GAAGGTCTCC AGAATGAAGG-3'; *Pdcd1* forward 5'-CTCGGCCATGGGA CGTAGGG-3', reverse, 5'-GGGTCTGCAGCATGCTAATG GCTG-3'; and *Gapdh* forward 5'-GCCTTCCGTGTTCCTAC CC-3', reverse, 5'-CAGTGGGCCCTCAGATGC-3'. PCR data were analyzed using CFX Manager 3.1 (BioRad). Experiments were performed in triplicates.

Purification of $CD8^+$ T Cells From Splenocytes

$CD8^+$ T cells were isolated from spleens of WT C57BL/6 mice by negative selection using the EasySep™ Mouse $CD8^+$ T cell isolation kit (Stem Cell Technologies) according to the manufacturer's protocol and cultured in complete media. Isolated $CD8^+$ T cells were activated with either plate-bound (1μg/mL) anti-CD3 and soluble (1μg/mL) anti-CD28, or Dynabeads™ Mouse T-Activator CD3/CD28 beads (Thermo Fischer Scientific) and co-cultured in the presence or absence of 50U/mL IL2, 50μM kynurenine (Sigma Aldrich), 3μM CH223191 (Sigma-Aldrich) or 10nM 2,3,7,8-tetrachlorodibenzo-p-dioxin (TCDD, Thomas Scientific).

Tumor Tissue Processing

Liberase Thermolysin Medium Research Grade solution (Roche) was used for the digestion of IE9mp1-mIDO and IE9mp1-EV tumor tissues harvested from WT C57BL/6 and IDOKO mice. Following digestion, direct *ex vivo* analysis by flow cytometry was performed in order to phenotype immune cell infiltration into the tumor. To lyse red blood cells in hemorrhagic tumor ascites fluids in order to perform phenotypic immune cell analysis, ACK lysis buffer was used. Ammonium-Chloride-Potassium (ACK) lysing buffer was added to ascites fluid and incubated at room temperature, then washed with 1x PBS before staining for surface and intracellular markers.

Cytokine and Chemokine Analysis

Cell-free tumor ascites fluid from IE9mp1-EV or IE9mp1-mIDO1 tumor-bearing WT C57BL/6 mice on Days 28 and 48 were harvest and analyzed for cytokines and chemokine levels using the 36-Plex Mouse ProcartaPlex Panel 1A Multiplex Luminex immunoassay kit (eBioscience). Data were collected using the Luminex-100 system and analyzed using StarStation Version 1.8 software (Applied Cytometry).

Confocal Microscopy

IE9mp1-mIDO1 or IE9mp1-Empty Vector tumor excised from WT C57BL/6 mice on Day 48 of tumor progression, or naïve $CD8^+$ T cells from WT C57BL/6 mice activated with anti-CD3/anti-CD28 and treated with kynurenine (50μM) or 2,3,7,8-tetrachlorodibenzo-p-dioxin (TCDD, 10nM) alone for 0 minutes, 30 minutes, 1 hour, 2 hours and 4 hours, were embedded in Tissue Freezing Medium (Ted Pella, Inc.) containing cryomolds

and immediately frozen in 2-methyl-butane (Sigma-Aldrich). 5μm frozen sections of the tissues were made using the cryostat and layered on Superfrost™ Plus Slides (Thermo Scientific). The slides were fixed in 4% para-formaldehyde for 15 minutes, washed and blocked for 60 minutes at room temperature. The slides were then stained for 3 hours at room temperature with mouse-specific antibodies anti-IDO (D7Z7U, Cell Signaling Technologies catalog no. 68572S), anti-CD8 (clone 53-6.7, BioLegend catalog no. 100702), anti-PD-1 (clone J43, BD Biosciences, catalog no. 551892), anti-AHR (clone W16012A, BioLegend, catalog no. 694502), and Hoechst 33342 nucleic acid stain (ThermoFisher Scientific, catalog no. H3570). Confocal analyses of stained slides were performed using a TCS SP8 Laser Scanning Spectral Confocal Microscope (LEICA Microsystems). For enumeration of cells positive for the individual markers, photographs of 10 fields (at 63x magnification) of stained tumors or cells were taken and each field was counted using ImageJ 1.74v software (NIH). Mean cell counts of total 10 fields were plotted. To ascertain AHR translocation to nucleus, Mean pixel intensity of AHR within the nucleus is calculated using Image J software.

Reagents and Internal Standards for High-Performance Liquid Chromatography (HPLC)

Sources for reagents were: HPLC-grade acetonitrile and water (Burdick & Jackson); mass spectrometry-grade formic acid and ammonium acetate (Sigma-Aldrich); calibration solution containing multiple calibrants in a solution of acetonitrile, trifluroacetic acid, and water (Agilent Technologies); metabolite standards and internal standards, including N-acetyl Aspartic acid-d3, Tryptophan-15N2, Sarcosine-d3, Glutamic acid-d5, Thymine-d4, Gibberellic acid, Trans-Zeatine, Jasmonic acid, 15N Anthranilic acid, and Testosterone-d3 (Sigma-Aldrich).

Sample Preparation for Mass Spectrometry and Metabolomics Analysis

Metabolites were extracted from cell lines and the extraction procedure was previously described (48). Briefly, mouse liver tissue pool was used as quality controls in the extraction procedure. The extraction step started with the addition of 750μL ice-cold methanol:water (4:1) containing 20μL spiked internal standards to each tissue and quality control samples. Ice-cold chloroform and water were added in a 3:1 ratio for a final proportion of 2:4:3 water:methanol:chloroform. The organic (methanol and chloroform) and aqueous layers were collected, dried and resuspended with 500μL of 50:50 methanol: water. The extract was deproteinized using a 3kDa molecular filter (Millipore Corporation) and the filtrate was dried under vacuum (Gardiner). Prior to mass spectrometry, the dried extracts were re-suspended in 100μL of injection solvent composed of 1:1 water:methanol and were subjected to liquid chromatography-mass spectrometry. The injection volume was 10μL.

Liquid Chromatography–Mass Spectrometry (LC-MS) Methods

For IDO pathway metabolites, ESI positive mode was used and analyzed using a 6495B triple quadrupole mass spectrometer (Agilent Technologies) coupled to a HPLC system (Agilent Technologies) *via* single reaction monitoring (SRM). Source parameters were gas temperature-290°C; gas flow 14L/min; nebulizer 20psi; sheath gas temperature 350°C; sheath gas flow 12L/min; capillary 3000V positive and 3000V negative; nozzle voltage 1500V positive and 1500V negative. Approximately 8–11 data points were acquired per detected metabolite. The HPLC column used was Zorbax eclipse XDB C-18, 1.8μm, 4.6×100mm (Agilent Technologies). Mobile phase A and B were 0.1% formic acid in water and acetonitrile respectively. Gradient used was: 0 min at 2% B; 2 min at 10% B, 12 min at 80% B, 18 min at 2% B followed by re-equilibration till end of the gradient 25 min to the initial starting condition (2% B). Flow rate used was 0.3mL/min. For purines and pyrimidines metabolites ESI positive mode was used and analyzed using a 6495B triple quadrupole mass spectrometer (Agilent Technologies) coupled to a HPLC system (Agilent Technologies) *via* single reaction monitoring (SRM). Source parameters, flow rate, and number of data points collected for purine/pyrimidines were similar to IDO pathway metabolites. A Waters X-bridge amide 3.5μm, 4.6×100mm column was used. Gradient used was: 0 min at 2% B; 6.50 min at 30% B; 7 min at 90% B; 12 min at 95%; 13 min at 2% B followed by re-equilibration till end of the gradient 20 min to the initial starting condition (2% B). The significance differences in levels of metabolites from various pathways between the IE9mp1-EV and -mIDO1 tumors and their importance are ascertained by p value (<0.05) and by impact score. The impact scores represent the importance of the metabolites in the metabolic network. They were calculated based on the centrality measures of a metabolite in a given metabolic network. Centrality is a local quantitative measure of the position of a node relative to the other nodes and is often used to estimate a node's relative importance or role in network organization. Specifically, we used relative betweenness centrality to calculate compound importance. The pathway impact is calculated as the sum of the importance measures of the matched metabolites normalized by the sum of the importance measures of all metabolites in each pathway (49).

Assay for Transposase Accessible Chromatin Sequencing (ATAC-seq)

50,000 isolated $CD8^+$ T cells were activated with Dynabeads™ Mouse T-Activator CD3/CD28 beads (Thermo Fischer Scientific), and co-cultured in the presence of 50μM kynurenine (Sigma-Aldrich) or 10nM TCDD (Thomas Scientific) for 2 or 28 hours, and ATAC-seq DNA libraries were prepared as previously described (38, 50). The final libraries were purified using AmpureXP beads, and validated for appropriate size on a 4200 TapeStation D1000 Screentape (Agilent Technologies). The DNA libraries were quantitated using KAPA Biosystems qPCR kit, and were pooled together in an equimolar fashion, following experimental design criteria.

Each pool was denatured and diluted to 350pM with 1% PhiX control library added. The resulting pool was then loaded into the appropriate NovaSeq Reagent cartridge for 100 cycle paired-end sequencing and sequenced on a NovaSeq6000 following the manufacturer's recommended protocol (Illumina). ATAC-seq data in raw FASTQ format were processed uniformly through ENCODE ATAC-seq pipeline version 1.4.0. The sequences in FASTQ file were aligned to mouse genome version mm10 using BOWTIE2 in Paired-end mode. The mitochondria reads, the duplicated reads and the reads with mapping quality less than 30 were removed from downstream analysis. Then MACS2 (–extsize73 –shift 37) was used to call accessible regions and to generate genome-wide insertion sites profiles for visualization. The insertion sites profile shows number of insertion events found in certain genomic location normalized by sequencing depth by million reads. ATAC-seq data quality was controlled by estimating signal-to-noise ratio, transcription start sites (TSS) enrichment, and enrichment in the universal DHS regions combined by ENCODE project.

Transcription Factor Binding Site Analysis

The core xenobiotic response element (XRE) sequence recognized by the AHR is 5'-T/GCGTG-3'. Position specific weight matrices (PWM) of XRE were extracted from the database TRANSFAC 7.0. The Transcription Element Search System (TESS) was used with default setting to search for AHR binding sites in the promoter region of each inhibitory gene (51).

Chromatin Immunoprecipitation Assay

Chromatin immunoprecipitation assay was performed on $CD8^+$ T cells activated with anti-CD3/anti-CD28 in the presence of kynurenine (50μM) or TCDD (10nM), using the EpiTect ChIP kit (Qiagen) according to the manufacturer's protocol. Cells were crosslinked in 1% formaldehyde at 37°C for 10 minutes. After chromatin shearing by sonication, the sheared chromatin was precleared with Protein A beads, and then incubated overnight with a purified anti-AHR antibody clone W16012A (BioLegend, catalog no. 694502) while rotating at 4°C. After DNA isolation and purification, the IP-DNA was quantified by real-time PCR. The following primer sequences were used for analysis of AHR binding to DNA: *Pdcd1* forward 5'-TATTTGAGGAAGGCATGAGC-3', reverse, 5'-TCTTAACACACACGCAATCC-3'.

Statistics

Flow cytometry, PCR, and confocal microscopy results are expressed as mean ± SEM and analyzed by two-tailed, Student's t-test, or one- and two-way ANOVA. Kaplan-Meier curves for survival analysis were analyzed by the Log-rank Test. Statistical significance was determined by a $p<0.05$. GraphPad Prism 7 software was used to perform analyses. The Metabolomics data was log2-transformed and normalized with internal standard per-sample, per-method basis. For every metabolite in the normalized dataset, two-sample t-tests were conducted to compare expression levels between different groups. Differential metabolites were identified by adjusting the p-values for multiple testing at an FDR<0.25 and generated a heat map. The transformed and normalized levels of metabolites were visualized by heat map. Metabolites were grouped by hierarchical clustering using Euclidean distances and complete linkage. Comparison of group means was performed by independent sample t-tests and two-way ANOVA. Metabolic pathways were obtained from Kyoto Encyclopedia of Genes and Genomes (KEGG) data base (52). The overall difference of groups of metabolites between conditions was analyzed by GlobalANCOVA. The Luminex measurement of cytokines and chemokines were log-transformed before analysis. For each mice strain, the mean levels of each group were compared by two-way ANOVA, with treatment group and time as the two factors. All tests were two-sided.

Study Approval

All animal experiments were carried out according to protocol guidelines reviewed and approved by the Institute Animal Care and Use Committee (IACUC) of Roswell Park Comprehensive Cancer Center (Buffalo, NY).

DATA AVAILABILITY STATEMENT

The original contributions presented in the study are included in the article/**Supplementary Material**. Further inquiries can be directed to the corresponding author.

ETHICS STATEMENT

The animal study was reviewed and approved by Roswell Park Comprehensive Cancer Center IACUC.

AUTHOR CONTRIBUTIONS

AA-M, RM, TT, FQ, R-YH, AL, and KO designed the experiments. AA-M and KO wrote the manuscript. AA-M performed the experiments and analyzed the data. RM designed, performed experiments, wrote, edited and reviewed, and revised the manuscript. TT designed the IDO expressing Cell line. VP and NP performed the metabolomics assay. PS performed genomic assays. AA-M, RM, HY, TL, JW, SB, and SL performed computational, bioinformatics, and statistical analyses. All authors contributed to the article and approved the submitted version.

ACKNOWLEDGMENTS

This work was supported by the National Cancer Institute (NCI) funded RPCI-UPCI Ovarian Cancer SPORE P50CA159981, NIH U24 CA232979, NIH R01 CA158318, NCI Cancer Center Support Grant P30 CA016056, NCI P30CA016056, NIH/NCI R01CA220297, and NIH/NCI R01CA216426 grants, and the use of Roswell Park Comprehensive Cancer Center's shared resources including the Flow Cytometry Core, Laboratory Animal Resource, Biostatistics Shared Resource, Bioinformatics

Shared Resource, and Genomics Shared Resource. We would like to thank Cheryl Eppolito for breeding animals used in this study, and the James N. Jarvis MD Lab at the University at Buffalo Jacobs School of Medicine and Biomedical Sciences for providing their expertise with the ATAC-seq experiment.

SUPPLEMENTARY MATERIAL

The Supplementary Material for this article can be found online at: https://www.frontiersin.org/articles/10.3389/fimmu.2021.678999/full#supplementary-material

REFERENCES

1. Torre LA, Trabert B, DeSantis CE, Miller KD, Samimi G, Runowicz CD, et al. Ovarian cancer statistics, 2018. *CA Cancer J Clin* (2018) 68(4):284–96. doi: 10.3322/caac.21456
2. Marcus CS, Maxwell GL, Darcy KM, Hamilton CA, McGuire WP. Current approaches and challenges in managing and monitoring treatment response in ovarian cancer. *J Cancer* (2014) 5(1):25–30. doi: 10.7150/jca.7810
3. Secord AA. Ovarian cancer: time to move beyond one size fits all. *Lancet Oncol* (2019) 20(6):754–5. doi: 10.1016/S1470-2045(19)30285-2
4. Sato E, Olson SH, Ahn J, Bundy B, Nishikawa H, Qian F, et al. Intraepithelial CD8+ tumor-infiltrating lymphocytes and a high CD8+/regulatory T cell ratio are associated with favorable prognosis in ovarian cancer. *Proc Natl Acad Sci USA* (2005) 102(51):18538–43. doi: 10.1073/pnas.0509182102
5. Zhang L, Conejo-Garcia JR, Katsaros D, Gimotty PA, Massobrio M, Regnani G, et al. Intratumoral T cells, recurrence, and survival in epithelial ovarian cancer. *N Engl J Med* (2003) 348(3):203–13. doi: 10.1056/NEJMoa020177
6. Ovarian Tumor Tissue Analysis C, Goode EL, Block MS, Kalli KR, Vierkant RA, Chen W, et al. Dose-Response Association of CD8+ Tumor-Infiltrating Lymphocytes and Survival Time in High-Grade Serous Ovarian Cancer. *JAMA Oncol* (2017) 3(12):e173290. doi: 10.1001/jamaoncol.2017.3290
7. Mellor AL, Keskin DB, Johnson T, Chandler P, Munn DH. Cells expressing indoleamine 2,3-dioxygenase inhibit T cell responses. *J Immunol* (2002) 168 (8):3771–6. doi: 10.4049/jimmunol.168.8.3771
8. Munn DH, Sharma MD, Baban B, Harding HP, Zhang Y, Ron D, et al. GCN2 kinase in T cells mediates proliferative arrest and anergy induction in response to indoleamine 2,3-dioxygenase. *Immunity* (2005) 22(5):633–42. doi: 10.1016/j.immuni.2005.03.013
9. Gandhi R, Kumar D, Burns EJ, Nadeau M, Dake B, Laroni A, et al. Activation of the aryl hydrocarbon receptor induces human type 1 regulatory T cell-like and Foxp3(+) regulatory T cells. *Nat Immunol* (2010) 11(9):846–53. doi: 10.1038/ni.1915
10. Mezrich JD, Fechner JH, Zhang X, Johnson BP, Burlingham WJ, Bradfield CA. An interaction between kynurenine and the aryl hydrocarbon receptor can generate regulatory T cells. *J Immunol* (2010) 185(6):3190–8. doi: 10.4049/jimmunol.0903670
11. Qian F, Villella J, Wallace PK, Mhawech-Fauceglia P, Tario JDJr., Andrews C, et al. Efficacy of levo-1-methyl tryptophan and dextro-1-methyl tryptophan in reversing indoleamine-2,3-dioxygenase-mediated arrest of T-cell proliferation in human epithelial ovarian cancer. *Cancer Res* (2009) 69(13):5498–504. doi: 10.1158/0008-5472.CAN-08-2106
12. Inaba T, Ino K, Kajiyama H, Yamamoto E, Shibata K, Nawa A, et al. Role of the immunosuppressive enzyme indoleamine 2,3-dioxygenase in the progression of ovarian carcinoma. *Gynecol Oncol* (2009) 115(2):185–92. doi: 10.1016/j.ygyno.2009.07.015
13. Okamoto A, Nikaido T, Ochiai K, Takakura S, Saito M, Aoki Y, et al. Indoleamine 2,3-dioxygenase serves as a marker of poor prognosis in gene expression profiles of serous ovarian cancer cells. *Clin Cancer Res* (2005) 11 (16):6030–9. doi: 10.1158/1078-0432.CCR-04-2671
14. Takao M, Okamoto A, Nikaido T, Urashima M, Takakura S, Saito M, et al. Increased synthesis of indoleamine-2,3-dioxygenase protein is positively associated with impaired survival in patients with serous-type, but not with other types of, ovarian cancer. *Oncol Rep* (2007) 17(6):1333–9. doi: 10.3892/or.17.6.1333
15. Qian F, Liao J, Villella J, Edwards R, Kalinski P, Lele S, et al. Effects of 1-methyltryptophan stereoisomers on IDO2 enzyme activity and IDO2-mediated arrest of human T cell proliferation. *Cancer Immunol Immunother CII* (2012) 61(11):2013–20. doi: 10.1007/s00262-012-1265-x
16. Holmgaard RB, Zamarin D, Munn DH, Wolchok JD, Allison JP. Indoleamine 2,3-dioxygenase is a critical resistance mechanism in antitumor T cell immunotherapy targeting CTLA-4. *J Exp Med* (2013) 210(7):1389–402. doi: 10.1084/jem.20130066
17. Kristeleit R, Davidenko I, Shirinkin V, El-Khouly F, Bondarenko I, Goodheart MJ, et al. A randomised, open-label, phase 2 study of the IDO1 inhibitor epacadostat (INCB024360) versus tamoxifen as therapy for biochemically recurrent (CA-125 relapse)-only epithelial ovarian cancer, primary peritoneal carcinoma, or fallopian tube cancer. *Gynecol Oncol* (2017) 146(3):484–90. doi: 10.1016/j.ygyno.2017.07.005
18. ClinicalTrials.gov Identifier: NCT02752074. *A Phase 3 Study of Pembrolizumab + Epacadostat or Placebo in Subjects With Unresectable or Metastatic Melanoma (Keynote-252 / ECHO-301)*. Available at: https://clinicaltrials.gov/ct2/show/NCT02752074 (Accessed March 26, 2019).
19. Long GV, Dummer R, Hamid O, Gajewski T, Caglevic C, Dalle S, et al. Epacadostat (E) plus pembrolizumab (P) versus pembrolizumab alone in patients (pts) with unresectable or metastatic melanoma: Results of the phase 3 ECHO-301/KEYNOTE-252 study. *J Clin Oncol* (2018) 36(15_suppl):108. doi: 10.2139/ssrn.3327362
20. Mullard A. IDO takes a blow. *Nat Rev Drug Discov* (2018) 17:307. doi: 10.1038/nrd.2018.67
21. Muller AJ, Manfredi MG, Zakharia Y, Prendergast GC. Inhibiting IDO pathways to treat cancer: lessons from the ECHO-301 trial and beyond. *Semin Immunopathol* (2019) 41(1):41–8. doi: 10.1007/s00281-018-0702-0
22. Matsuzaki J, Gnjatic S, Mhawech-Fauceglia P, Beck A, Miller A, Tsuji T, et al. Tumor-infiltrating NY-ESO-1-specific CD8+ T cells are negatively regulated by LAG-3 and PD-1 in human ovarian cancer. *Proc Natl Acad Sci USA* (2010) 107(17):7875–80. doi: 10.1073/pnas.1003345107
23. Opitz CA, Litzenburger UM, Sahm F, Ott M, Tritschler I, Trump S, et al. An endogenous tumour-promoting ligand of the human aryl hydrocarbon receptor. *Nature* (2011) 478(7368):197–203. doi: 10.1038/nature10491
24. Huang RY, Eppolito C, Lele S, Shrikant P, Matsuzaki J, Odunsi K. LAG3 and PD1 co-inhibitory molecules collaborate to limit CD8+ T cell signaling and dampen antitumor immunity in a murine ovarian cancer model. *Oncotarget* (2015) 6(29):27359–77. doi: 10.18632/oncotarget.4751
25. Roby KF, Taylor CC, Sweetwood JP, Cheng Y, Pace JL, Tawfik O, et al. Development of a syngeneic mouse model for events related to ovarian cancer. *Carcinogenesis* (2000) 21(4):585–91. doi: 10.1093/carcin/21.4.585
26. Jiao L, Maity S, Coarfa C, Rajapakshe K, Chen L, Jin F, et al. A Prospective Targeted Serum Metabolomics Study of Pancreatic Cancer in Postmenopausal Women. *Cancer Prev Res (Phila)* (2019) 12(4):237–46. doi: 10.1158/1940-6207.CAPR-18-0201
27. Badawy AA. Kynurenine Pathway of Tryptophan Metabolism: Regulatory and Functional Aspects. *Int J Tryptophan Res* (2017) 10:1178646917691938. doi: 10.1177/1178646917691938
28. Ishidoh K, Kamemura N, Imagawa T, Oda M, Sakurai J, Katunuma N. Quinolinate phosphoribosyl transferase, a key enzyme in de novo NAD(+) synthesis, suppresses spontaneous cell death by inhibiting overproduction of active-caspase-3. *Biochim Biophys Acta* (2010) 1803(5):527–33. doi: 10.1016/j.bbamcr.2010.02.007
29. Fallarino F, Grohmann U, You S, McGrath BC, Cavener DR, Vacca C, et al. The combined effects of tryptophan starvation and tryptophan catabolites down-regulate T cell receptor zeta-chain and induce a regulatory phenotype in naive T cells. *J Immunol* (2006) 176(11):6752–61. doi: 10.4049/jimmunol.176.11.6752
30. Cook DB, McLucas BC, Montoya LA, Brotski CM, Das S, Miholits M, et al. Multiplexing protein and gene level measurements on a single Luminex platform. *Methods* (2019) 158:27–32. doi: 10.1016/j.ymeth.2019.01.018
31. Bystry RS, Aluvihare V, Welch KA, Kallikourdis M, Betz AG. B cells and professional APCs recruit regulatory T cells via CCL4. *Nat Immunol* (2001) 2 (12):1126–32. doi: 10.1038/ni735
32. Kumar V, Patel S, Tcyganov E, Gabrilovich DI. The Nature of Myeloid-Derived Suppressor Cells in the Tumor Microenvironment. *Trends Immunol* (2016) 37(3):208–20. doi: 10.1016/j.it.2016.01.004

33. Lesokhin AM, Hohl TM, Kitano S, Cortez C, Hirschhorn-Cymerman D, Avogadri F, et al. Monocytic CCR2(+) myeloid-derived suppressor cells promote immune escape by limiting activated CD8 T-cell infiltration into the tumor microenvironment. *Cancer Res* (2012) 72(4):876–86. doi: 10.1158/0008-5472.CAN-11-1792
34. Murray IA, Morales JL, Flaveny CA, Dinatale BC, Chiaro C, Gowdahalli K, et al. Evidence for ligand-mediated selective modulation of aryl hydrocarbon receptor activity. *Mol Pharmacol* (2010) 77(2):247–54. doi: 10.1124/mol.109.061788
35. Whitlock JP Jr. Induction of cytochrome P4501A1. *Annu Rev Pharmacol Toxicol* (1999) 39:103–25. doi: 10.1146/annurev.pharmtox.39.1.103
36. Kanno Y, Miyama Y, Takane Y, Nakahama T, Inouye Y. Identification of intracellular localization signals and of mechanisms underlining the nucleocytoplasmic shuttling of human aryl hydrocarbon receptor repressor. *Biochem Biophys Res Commun* (2007) 364(4):1026–31. doi: 10.1016/j.bbrc.2007.10.140
37. Reyes H, Reisz-Porszasz S, Hankinson O. Identification of the Ah receptor nuclear translocator protein (Arnt) as a component of the DNA binding form of the Ah receptor. *Science* (1992) 256(5060):1193–5. doi: 10.1126/science.256.5060.1193
38. Buenrostro JD, Giresi PG, Zaba LC, Chang HY, Greenleaf WJ. Transposition of native chromatin for fast and sensitive epigenomic profiling of open chromatin, DNA-binding proteins and nucleosome position. *Nat Methods* (2013) 10(12):1213–8. doi: 10.1038/nmeth.2688
39. Zhao B, Degroot DE, Hayashi A, He G, Denison MS. CH223191 is a ligand-selective antagonist of the Ah (Dioxin) receptor. *Toxicol Sci* (2010) 117 (2):393–403. doi: 10.1093/toxsci/kfq217
40. Uyttenhove C, Pilotte L, Theate I, Stroobant V, Colau D, Parmentier N, et al. Evidence for a tumoral immune resistance mechanism based on tryptophan degradation by indoleamine 2,3-dioxygenase. *Nat Med* (2003) 9(10):1269–74. doi: 10.1038/nm934
41. Liu Y, Liang X, Dong W, Fang Y, Lv J, Zhang T, et al. Tumor-Repopulating Cells Induce PD-1 Expression in CD8(+) T Cells by Transferring Kynurenine and AhR Activation. *Cancer Cell* (2018) 33(3):480–94 e7. doi: 10.1016/j.ccell.2018.02.005
42. Tullius SG, Biefer HR, Li S, Trachtenberg AJ, Edtinger K, Quante M, et al. NAD+ protects against EAE by regulating CD4+ T-cell differentiation. *Nat Commun* (2014) 5:5101. doi: 10.1038/ncomms6101
43. Zhou L. AHR Function in Lymphocytes: Emerging Concepts. *Trends Immunol* (2016) 37(1):17–31. doi: 10.1016/j.it.2015.11.007
44. Eleftheriadis T, Pissas G, Liakopoulos V, Stefanidis I. IDO decreases glycolysis and glutaminolysis by activating GCN2K, while it increases fatty acid oxidation by activating AhR, thus preserving CD4+ Tcell survival and proliferation. *Int J Mol Med* (2018) 42(1):557–68. doi: 10.3892/ijmm.2018.3624
45. Bianchi-Smiraglia A, Bagati A, Fink EE, Affronti HC, Lipchick BC, Moparthy S, et al. Inhibition of the aryl hydrocarbon receptor/polyamine biosynthesis axis suppresses multiple myeloma. *J Clin Invest* (2018) 128(10):4682–96. doi: 10.1172/JCI70712
46. Patel MR, Chang YF, Chen IY, Bachmann MH, Yan X, Contag CH, et al. Longitudinal, noninvasive imaging of T-cell effector function and proliferation in living subjects. *Cancer Res* (2010) 70(24):10141–9. doi: 10.1158/0008-5472.CAN-10-1843
47. Tomihara K, Guo M, Shin T, Sun X, Ludwig SM, Brumlik MJ, et al. Antigen-specific immunity and cross-priming by epithelial ovarian carcinoma-induced CD11b(+)Gr-1(+) cells. *J Immunol* (2010) 184(11):6151–60. doi: 10.4049/jimmunol.0903519
48. Vantaku V, Dong J, Ambati CR, Perera D, Donepudi SR, Amara CS, et al. Multi-omics Integration Analysis Robustly Predicts High-Grade Patient Survival and Identifies CPT1B Effect on Fatty Acid Metabolism in Bladder Cancer. *Clin Cancer Res* (2019) 25(12):3689–701. doi: 10.1158/1078-0432.CCR-18-1515
49. Xia J, Wishart DS. MetPA: a web-based metabolomics tool for pathway analysis and visualization. *Bioinformatics* (2010) 26(18):2342–4. doi: 10.1093/bioinformatics/btq418
50. Buenrostro JD, Wu B, Chang HY, Greenleaf WJ. ATAC-seq: A Method for Assaying Chromatin Accessibility Genome-Wide. *Curr Protoc Mol Biol* (2015) 109:21.29.1–9. doi: 10.1002/0471142727.mb2129s109
51. Schug J. Using TESS to Predict Transcription Factor Binding Sites in DNA Sequence. *Curr Protoc Bioinf* (2008) 21(1):2.6.1–15. doi: 10.1002/0471250953.bi0206s21
52. Kanehisa M, Goto S. KEGG: kyoto encyclopedia of genes and genomes. *Nucleic Acids Res* (2000) 28(1):27–30. doi: 10.1093/nar/28.1.27

Conflict of Interest: KO is a co-founder of Tactiva Therapeutics and receives research support from AstraZeneca and Tesaro.

The remaining authors declare that the research was conducted in the absence of any commercial or financial relationships that could be construed as a potential conflict of interest.